International Journal of Engineering

Journal Homepage: www.ije.ir

Experimental Study to Evaluate Antisymmetric Reinforced Concrete Deep Beams with Openings under Concentrated Loading Using Strut and Tie Model

A. S. J. Al-Zuheriy*

Civil Engineering Department, University of Technology – Iraq, Baghdad, Iraq

P A P E R I N F O

Paper history:
Received 07 September 2023
Received in revised form 04 October 2023
Accepted 05 October 2023

Keywords:
Strut-and-Tie Models
Crack Patterns
Load Deflection Analysis
Concentrated Loading
Strut Reinforcement
Deep Beams

A B S T R A C T

The Strut-and-Tie modeling (STM) technique represents an applicable and valuable method for structural engineers to design disturbed regions (D-regions) of reinforced concrete structures where the assumption of plane sections remaining plane after loading is inapplicable. The most important aspect to guarantee the suitable structural and economic performance of the design is finding a suitable truss-analogy model, leading to the use of a more efficient model in structural buildings. The evaluation of the antisymmetric Strut-and-Tie models (STM) with openings under different concentrated external loads has not been comprehensively investigated in the literature. So, to address this gap, the goal of this paper is to achieve the most efficient reinforcement layout design in antisymmetric reinforced concrete deep beams with openings under concentrated loading using the strut and tie model. The experimental work was conducted and included (3) antisymmetric reinforced concrete deep beams with openings that were tested under different concentrated loadings (25, 35, and 16 kips for Specimens 1, 2, and 3, respectively) using the strut and tie model. The ANSYS FEM software is used for the initial strut and tie analysis, and the RISA-3D structural analysis program is used to find the internal forces for all members under concentrated external loads in each specimen. The findings of this paper show that Specimen 1 had the highest efficiency of 1.67, while Specimen 3 had the lowest efficiency of 1.31. It can be concluded that the efficient reinforcement layout of the strut and tie model leads to the highest efficiency of the model, regardless of the value of the externally applied load.

***doi**: 10.5829/ije.2023.36.12c.17*

Graphical Abstract

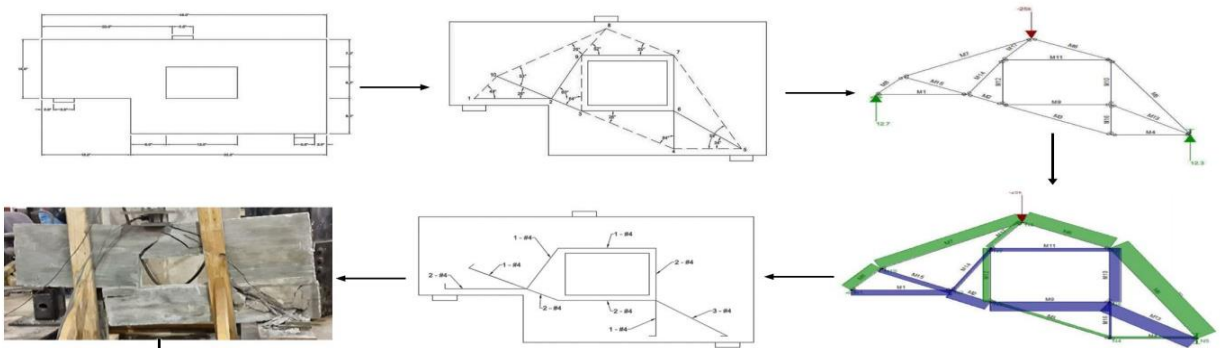

Load/weight ratio efficiencies for each specimen

Group	Reinforcement (lb)	Ultimate Load (kips)	Design Load (kips)	Deflection at Ultimate (in)	Efficiency (kips/lb)
1	13.17	22	25	0.14	1.67
2	19.767	29.297	35	0.22	1.48
3	13.51	17.75	16	0.34	1.31

*Corresponding Author Email: ahmed.sh.jeber@uotechnology.edu.iq (A. S. J. Al-Zuheriy)

Please cite this article as: A. S. J. Al-Zuheriy, Experimental Study to Evaluate Antisymmetric Reinforced Concrete Deep Beams with Openings under Concentrated Loading Using Strut and Tie Model, ***International Journal of Engineering, Transactions C: Aspects***, Vol. 36, No. 12, (2023), 2272-2283

1. INTRODUCTION

Overall, in the world, reinforced concrete structures have been utilized in a wide range of ways. The safe and economical design of reinforced concrete structures is always an important challenge for civil engineers, especially since their point of view is oriented toward developing a sustainable world. In general, reinforced concrete structures are divided into two main groups based on their behavior under loading: the Bernoulli group (B-group), which has linear strain distributions, for example, all the standard and commonly structural concrete members, and the Disturbed group (D-group), which has nonlinear strain distributions, for instance, the nonstandard or unconventional structural concrete members (Strut-and-Tie models) (STM). The main reasons for the nonlinear strain distribution are the low slenderness and geometrical discontinuities. To select accurate, effective, and reasonable methods for design, the nonlinearity and discontinuity of the D-group members represent big challenges for civil engineers. For over two decades and among many methods, the strut-and-tie modeling (STM) method has been utilized in a wide range to design the D-group of reinforced concrete members [1]. Building code requirements for standard and commonly used structural concrete members have been part of the design codes for quite some time. However, the design codes previously had little guidance on designing nonstandard or unconventional members. To account for these nonstandard members, design codes have included guidelines for the design of such members by incorporating a strut and tie model design approach. Over the years, tests and research have been performed on the strut and tie model designs to be recommended and implemented into the various design codes [1-6].

At the end of the nineteenth century and the beginning of the twentieth century, Ritter [7] and Mörsch [8] proposed the STM method, which is a truss-like method leading to simplifying the complex force transfer mechanism. Schlaich et al. [9] presented a comprehensive work on the strut-and-tie modeling techniques, leading to an extensive investigation of using this method. Further research to generalize this method as a consistent design method was done by Schlaich and Schäfer [10]. After that, a lot of researchers studied and reported many different types of techniques and algorithms related to the strut-and-tie modeling (STM) technique. An evolutionary structural optimization method was demonstrated by Xie and Steven [11]. This method worked on creating strut-and-tie models by optimization of the topology. As well as based on Xie and Steven [11], Yang et al. [12] developed a bidirectional evolutionary optimization method. Then, Liang et al. [13, 14] proposed a performance-based optimization method for strut-and-tie modeling. In the first decade of the twenty-first century, many researchers [15-20] introduced the important developments of the strut-and-tie modeling technique and experienced different types of algorithms to develop this method.

In the second decade of the twenty-first century, the strut-and-tie modeling (STM) technique was developed, and new procedures were performed for strut-and-tie modeling through the established full homogenization optimization method [21], the smooth evolutionary structural optimization method [22], and the hybrid technique combining different methods [23-25]. El-Metwally and Chen [26] proposed a method that requires an equilibrium of the axial force while neglecting the compatibility of strain. In the STM method, the cracking of concrete and compatibility conditions were implemented to predict the ultimate behavior of concrete structures [27]. Many researchers conducted experimental work on various STM designs to validate their effectiveness and safety [28]. The effect of loading during an earthquake has been investigated in the literature [29, 30]. In respect of each load combination, a basis is created based on their previously proposed generation methods, the optimization-based Strut-and-Tie models (OPT-STMs), which resulted in economical and safe designs compared to traditional models [31-33]. A seismic vulnerability index methodology was improved to be used uniformly in reinforced concrete structures overall the world according to the earthquake design principles [34, 35]. The reinforced high-strength concrete beams' structural behavior was numerically investigated by Jabbar et al. [36]. The article introduced an experimental study to estimate an equation for accounting for deflection in reinforced concrete beams by utilizing the shear steel plates as a stirrup [37]. By employing a suitable strut-and-tie model, the results of experimental work on deep beam concrete samples consisting of recycled aggregates were introduced by Chaudhari and Suryawanshi [38].

Over the years, tests and research have been performed on the different strut-and-tie model designs. As a result of the literature review, this study is considered unique from previous research because no other study has attempted to investigate and evaluate the antisymmetric reinforced concrete deep beams with openings under concentrated loading using the strut and tie model. The goal of the paper is to achieve the most efficient reinforcement layout design (this was evaluated by the load capacity to the total steel weight ratio) among the three strut-and-tie models (STM) that are used in the antisymmetric reinforced concrete deep beams. To achieve this goal, the experimental work was conducted and included (3) antisymmetrically reinforced concrete deep beams with openings that were tested under different concentrated loading using the strut and tie model. The 3 unconventional concrete members (antisymmetric reinforced concrete deep beams with openings) were poured and tested under different

concentrated external loads equal to 25, 35, and 16 kips for Specimens 1, 2, and 3, respectively.

2. EXPERIMENTAL WORK

The experimental work included (3) antisymmetric reinforced concrete deep beams with openings that were tested under different concentrated loads using the Strut and Tie Model with 4,500 psi as the nominal compressive strength. All the samples had a width of 48 inches and a height of 24 inches. The beam's effective depth is 3.5 inches. The 3 unconventional concrete members (antisymmetric reinforced concrete deep beams with openings) were poured and tested under different concentrated external loads equal to 25, 35, and 16 kips for Specimens 1, 2, and 3, respectively. The following describes the experimental work performed for this paper.

2. 1. Initial Guidelines The geometry of the unconventional concrete member is shown in Figure 1. The work involved designing the steel reinforcement without load or phi factors. It was originally assumed that the concrete strength was 4,500 psi for the design and analysis of the strut and tie model. Figures 2 and 3 are images of the stress profile created using the ANSYS FEM software. Figure 2 is a contour of the stresses in the concrete member with a certain load. Figure 3 shows arrows oriented in the direction of the stresses distributed along the member. These FEM results were used for the initial strut and tie analysis.

2. 2. STM Analysis After the ANSYS analysis was performed, several strut and tie models were designed and analyzed by considering tension and compression zones. The bottom left corner of the central opening was the critical tension part; therefore, constraints in this zone were addressed by adding tie bars. Figure 4 is the final strut and tie model design that was used for the final reinforcement layout. The design in Figure 4 shows the location of all struts and ties with the corresponding

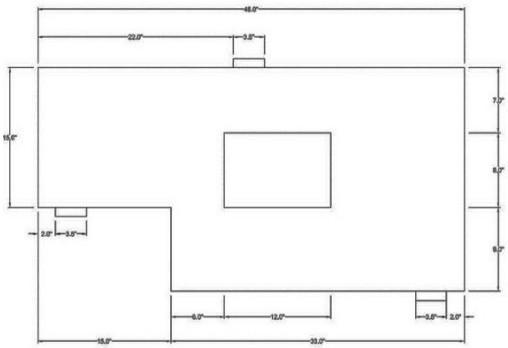

Figure 1. The geometry of the unconventional reinforced concrete member

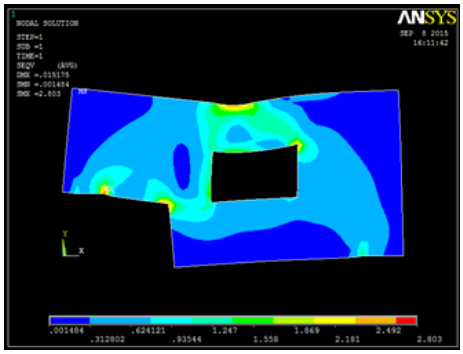

Figure 2. The contour of the stresses in the concrete member using ANSYS

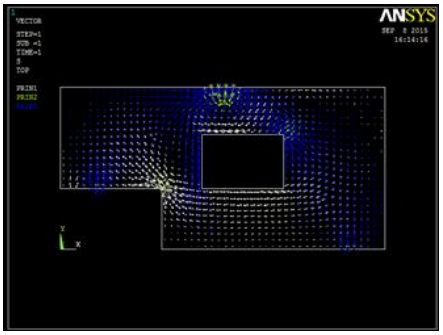

Figure 3. Arrows demonstrating the stress orientation of the concrete obtained with ANSYS

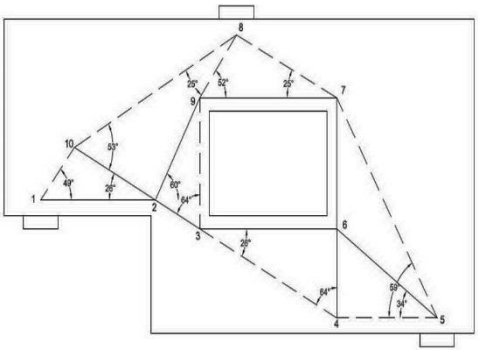

Figure 4. Strut and tie design

angles for each. All strut and tie angles are within the allowable limits of 25° and 65°. A cover of 1.2 inches was given along the supports and 1 inch of cover was given around the central opening of the concrete member. The lengths of the strut and ties can be seen in Table 1.

After the strut and tie model was designed using ANSYS, the model was analyzed using the RISA-3D structural analysis program to find the internal forces for all members under a concentrated external load equal to 25 kips. Figure 5 shows the members and nodes. Figure 6 shows the reaction forces at each support. Figure 7 shows the compression (struts) members, which are depicted in green, and the tension members (ties), depicted in blue.

TABLE 1. Member length of struts and ties between nodes

Member	Node	Length (in)
M1	1-2	11.72
M2	2-3	5.04
M3	3-4	15.56
M4	4-5	10.25
M5	5-7	19.68
M6	7-8	11.32
M7	8-10	18.64
M8	1-10	5.30
M9	3-6	14.00
M10	6-7	10.00
M11	7-9	14.00
M12	3-9	10.00
M13	5-6	12.30
M14	2-9	9.02
M15	2-10	9.19
M16	4-6	6.80
M17	8-9	6.09

*Light gray member denotes tension tie

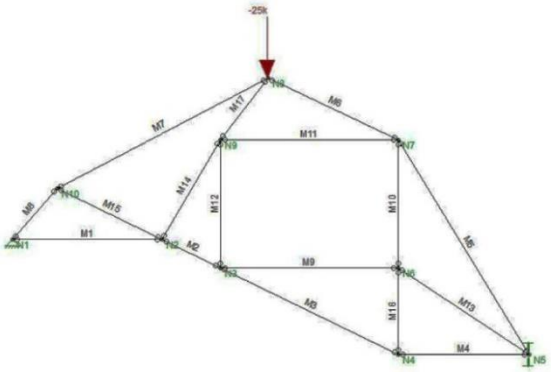

Figure 5. Strut and tie design imputed into RISA with a design load of 25 kips for force analysis

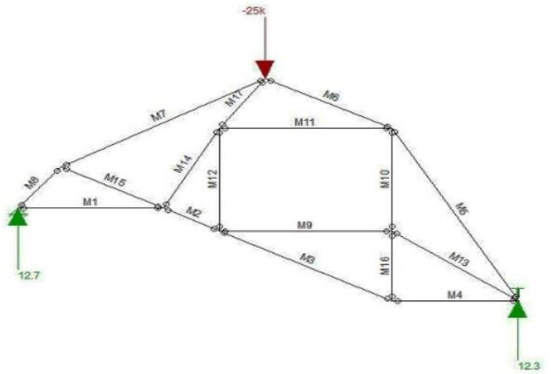

Figure 6. Support reactions were obtained from RISA using a 25-kip load for the strut and tie model

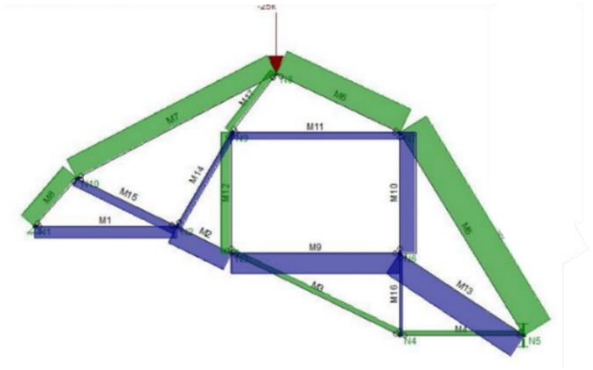

Figure 7. Member forces for the strut and tie design with 25 kips. Compression members are depicted in green, while tension members are in blue

2. 3. STM Rebar Design Once the strut and tie model was created, it was focused on maximizing the efficiency of the steel rebar layout for the specimen. Axial forces for the members of the strut and tie model were found from a 25 kip loading through the RISA model. These values were used as a baseline to interpolate axial forces from 10 to 30 kip as stated in Table 2. Using these calculations, the amount of required steel was calculated using Equation (1).

$$A_{s,req.} = \frac{T}{fy} \quad (1)$$

The required area of steel was used to find the number of required steel rebars. The calculation was considered for No. 2, 3, and 4 bars. The volume of steel for each bar was calculated using the lengths between nodes and the cross-sectional area of the different rebar sizes. The most efficient loading for each bar was calculated as a tensile force/volume value, as stated in Table 3. The highest value was found to be an efficiency of 0.94 kips/volume for the 25-kip loading. To ensure the width of the struts and ties throughout the model would not exceed the dimensions of the specimen, a strut and tie width analysis was performed. To determine the width of the struts/ties, the strength of each node, f_{cn}, and the strength of each strut, f_{cs}, were found. The following equations were used to determine the strength of the nodes and struts:

$$f_{cn} = 0.85 * \beta_n * f'c \quad (2)$$

$$f_{cs} = 0.85 * \beta_s * f'c \quad (3)$$

The β_n and β_s factors are based on the axial forces applied at each node. The fewer tensile forces acting on a node, the stronger that node will be. There are no defined values for the β_n or β_s factors for a T-T-T (Tension-Tension-Tension) node, therefore, it was assumed to be a C-T-T (Compression-Tension-Tension) node. Table 4 presents the strength of each strut and node. Once the strengths of the nodes and struts were determined for each node the two values were compared. The lower value of f_{cn} and f_{cs} for each node was used as

TABLE 2. Axial forces in struts and ties under design loads

Load (kips)	10	11	12	13	14	15	16	17	18	19	20	21	22	23	24	25	26	27	28	29	30
Members	**Axial Force (kips)**																				
M1	-4.36	-4.79	-5.23	-5.66	-6.1	-6.53	-6.97	-7.41	-7.84	-8.28	-8.71	-9.15	-9 58	-10.02	-10.45	-10.8	-11.33	-11.76	-12.2	-12.63	-13.07
M2	-6.88	-7.56	-8 25	-8.94	-9.63	-10.31	-11	-11.69	-12.38	-13.06	-13.75	-14.44	-15.13	-15.81	-16.5	-17.19	-17.88	-18.57	-19.25	-19.94	-20.63
M3	1.84	2.02	2.2	2.39	2.57	2.75	2.94	3.12	3.3	3.49	3.67	3.86	4.04	4.22	4.41	4.59	4.77	4.96	5.14	5.32	5.51
M4	1.66	1.82	1.99	2.15	2.32	2.48	2.65	2.82	2.98	3.15	3.31	3.48	3.64	3.81	3.97	4.14	4.31	4.47	4.64	4.8	4.97
M5	11.88	13.06	14.25	15.44	16.63	17.81	19	20.19	21.38	22.56	23.75	24.94	26.13	27.31	28.5	29.69	30.88	32.07	33.25	34.44	35.63
M6	9.75	10.73	11.7	12.68	13.65	14.63	15.6	16.58	17.55	18.53	19.5	20.48	21.45	2.43	23.4	24.38	25.36	26.33	27.31	28.28	26
M7	8.05	8.85	9.66	10.46	11.27	12.07	12.88	13.68	14.49	15.29	16.1	16.9	17.71	18.51	19.32	20.12	20.92	21.73	22.53	23.34	24.14
M8	6.68	7.35	8.02	8.68	9.35	10.02	10.69	11.36	12.02	12.69	13.36	14.03	14.7	15.36	16.03	16.7	17.37	18.04	18.7	19.37	20.04
M9	-7.84	-8.62	-9.4	-10.19	-10.97	-11.75	-12.54	-13.32	-14.1	-14.89	-15.67	-16.46	-17.24	-18.02	-18.18	-19.59	-20.37	-21.16	-21.94	-22.72	-23.51
M10	-6	-6.6	-7.2	-7.81	-8.41	-9.01	-9.61	-10.21	-10.81	-11.41	-12.01	-12.61	-13.21	-13.81	-14.41	-15.01	-15.61	-16.21	-16.81	-17.41	-18.01
M11	-2.64	-2.91	-3.17	-3.44	-3.7	-3.97	-4.23	-4.49	-4.76	-5.02	-5.29	-5.55	-5.82	-6.08	-6.35	-6.61	-6.87	-7.14	-7.4	-7.67	-7.93
M12	3.8	4.18	4.56	4.95	5.33	5.71	6.09	6.47	6.85	7.23	7.61	7.99	8.37	8.75	9.13	9.51	9.89	10.27	10.65	11.03	11.41
M13	-9.41	-10.35	-11.29	-12.23	-13.17	-14.11	-15.05	-15.99	-16.93	-17.88	-18.82	-19.76	-20.7	-21.64	-22.58	-23.52	-24.46	-25.4	-26.34	-27.28	-28.22
M14	-1.9	-2.09	-2.28	-2.48	-2.67	-2.86	-3.05	-3.24	-3.43	-3.62	-3.81	-4	-4.19	-4.38	-4.57	-4.76	-4.95	-5.14	-5.33	-5.52	-5.71
M15	-3.1	-3 41	-3.72	4-.03	-4.34	-4.65	-4.96	-5.27	-5.58	-5.89	-6.2	-6.51	-6.82	-7.13	-7.44	-7.75	-8.06	-8.37	-8.68	-8.99	-9.3
M16	-0.8	-0.88	-0.96	-1.05	-1.13	-1.21	-1.29	-1.37	-1 45	-1.53	-1.61	-1.69	-1.77	-1.85	-1.93	-2.01	-2.09	-2.17	-2.25	-2.33	-2.41
M17	2.74	3.01	3.29	3.56	3.84	4.11	4.38	4.66	4.93	5.21	5.48	5.75	6.03	6.3	6.58	6.85	7.12	7.4	7.67	7.95	8.22

*Light gray member denotes tension tie

TABLE 3. Load/Volume efficiency calculations for tension ties under design loads

Load (kips)	10	11	12	13	14	15	16	17	18	19	20	21	22	23	24	25	26	27	28	29	30
Member	**Volume #2 bars (in^3)**																				
M1	1.149	1.723	1.723	1.723	1.723	1 723	2.297	2.297	2.297	2.297	2.297	2.872	2.872	2.872	2.872	2.872	3.446	3.446	3.446	3.446	3.446
M2	0.987	0.987	0.987	1.234	1.234	1.234	1.234	1.480	1.480	1.480	1.727	1.727	1.727	1.974	1.974	1.974	2.220	2.220	2.220	2.467	2.467
M9	2.744	2.744	3.430	3.430	3.430	4.116	4.116	4.802	4.802	4.802	5.488	5.488	5.488	6.174	6.174	6.174	6.860	6.860	6.860	7.546	7.546

M 10	1.470	1.470	1.470	1.960	1.960	1.960	2.450	2.450	2.450	2.450	2.450	2.940	2.940	2.940	2.940	2.940	3.430	3.430	3.920	3.920	3.920	3.920	3.920	4.410					
M11	1.372	1.372	1.372	1.372	1.372	1.372	1.372	1.372	2.058	2.058	2.058	2.058	2.058	2.058	2.058	2.058	2.058	2.058	2.744	2.744	2.744	2.744	2.744	2.744					
M 13	3.014	3.014	3.014	3.616	3.616	3.616	4.219	4.219	4.822	4.822	4.822	5.425	5.425	5.425	6.027	6.027	6.630	6.630	7.233	7.233	7.233	7.233	7.835	7.835					
M 14	0.442	0.442	0.442	0.884	0.884	0.884	0.884	0.884	0.884	0.884	0.884	0.884	0.884	0.884	0.884	0.884	1.326	1.326	1.326	1.326	1.326	1.326	1.326	1.326					
M 15	0.901	0.901	0.901	0.901	0.901	0.901	1 351	0.351	1.351	1.351	1.351	0.351	1.351	0.351	0.801	1.801	1.801	1.801	1.801	1.801	1.801	1.801	2.251	2.251					
M 16	0.333	0.333	0.333	0.333	0.333	0.333	0.333	0.333	0.333	0.333	0.333	0.333	0.333	0.333	0.333	0.333	0.333	0.333	0.333	0.333	0.333	0.666	0.666	0.666					
Total Volume	12.411	12.985	15.206	15.452	15.452	17.681	18.256	20.477	20.477	21.570	22.503	23.077	24.130	25.553	26.597	26.597	29.883	29.883	30.216	32.202	34.689	34.135	34.135	34.689					
Load/Volume	0.806	0.847	0.789	0.841	0.906	0.848	0.876	0.830	0.879	0.881	0.889	0.910	0.912	0.900	0.902	0.940	0.870	0.904	0.927	0.901	0.918	0.820	0.836	0.865					
Load (kips)	10	11	12	13	14	15	16	17	18	19	20	21	22	23	24	25	26	27	28	29	30	27	28	29					
Member	**Volume #3 bars (in^3)**																												
M1	1.289	1 289	2.579	2.579	2.579	2.579	2.579	2.579	2.579	2.579	2.579	2.579	2.579	3.868	3.868	3.868	3.868	3.868	3.868	3.868	3.868	3.868	3.868	3.868					
M2	1.108	1.108	1.108	1.108	1.108	1.662	1.662	1.662	0.662	1.662	1.662	1.662	2.215	2.215	2.215	2.215	2.215	2.215	2.215	2.215	2.769	7.700	7.700	7.700					
M9	3.080	3.080	3.080	4.620	4.620	4.620	4.620	4.620	4.620	6.160	6.160	6.160	6.160	6.160	6.160	6.160	7.700	7.700	7.700	7.700	7.700	4.400	4.400	4.400					
M 10	2.200	2.200	2.200	2.200	2.200	2.200	2.200	3.300	3.300	3.300	3.300	3.300	3.300	3.300	3.300	4.400	4.400	4.400	4.400	4.400	4.400	3.080	3.080	3.080					
M11	1.540	1.540	1.540	1.540	1.540	1.540	1.540	1.540	1.540	3.080	3.080	3.080	3.080	3.080	3.080	3.080	6.765	6.765	6.765	8.118	8.118	8.118	8.118	8.118					
M 13	2.706	4.059	4.059	4.059	4.059	4.059	5.412	5.412	5.412	5.412	5.412	5.412	6.765	6.765	6.765	6.765	8.118	8.118	8.118	8.118	8.118	1.984	1.984	1.984					
M 14	0.992	0.992	0.992	0.992	0.992	0.992	0.992	0.992	0.992	0.992	0.992	0.992	0.992	0.992	0.992	0.992	1.984	1.984	1.984	1.984	1.984	2.022	2.022	2.022					
M 15	1.011	1.011	1.011	1.011	1.011	1.011	2.022	2.022	2.022	2.022	2.022	2.022	2.022	2.022	2.022	2.022	2.022	2.022	2.022	2.022	2.022	0.748	0.748	0.748					
M 16	0.748	0.748	0.748	0.748	0.748	0.748	0.748	0.748	0.748	0.748	0.748	0.748	0.748	0.748	0.748	0.748	0.748	0.748	0.748	0.748	0.748	34.135	34.135	34.689					
Total Volume	14.674	16.027	17.316	18.856	18.856	19.410	21.774	22.874	22.874	25.954	25.954	25.954	27.861	29.150	29.150	30.250	32.782	34.135	34.135	34.689	34.689	29.150	29.150	30.250					
Load/Volume	0.681	0.686	0.693	0.689	0.742	0.773	0.735	0.743	0.787	0.732	0.771	0.809	0.790	0.789	0.823	0.826	0.793	0.791	0.820	0.836	0.865	0.823	0.826	0.826					
Load (kips)	10	11	12	13	14	15	16	17	18	19	20	21	22	23	24	25	26	27	28	29	30	24	25	26					
Member	**Volume #4 bars (in^3)**																												

M1	2.344	2.344	2.344	2.344	2.344	2.344	2.344	2.344	2.344	2.344	2.344	2.344	2.344	4.688	4.688	4.688	4.688	4.688	4.688	4.688	4.688	4.688	4.688
M2	1.007	1.007	1.007	0.007	2.014	2.014	2.014	2.014	2.014	2.014	2.014	2.014	2.014	2.014	2.014	2.014	2.014	2.014	2.014	3.021	3.021	3.021	3.021
M9	2.800	2.800	5.600	5.600	5.600	5.600	5.600	5.600	5.600	5.600	5.600	5.600	5.600	5.600	5.600	8.400	8.400	8.400	8.400	8.400	8.400	8.400	8.400
M 10	2.000	2.000	2.000	2.000	2.000	4.000	4.000	4.000	4.000	4.000	4.000	4.000	4.000	4.000	4.000	4.000	4.000	4.000	4.000	4.000	4.000	4.000	6.000
M11	2.800	2.800	2.800	2.800	2.800	2.800	2.800	2.800	2.800	2.800	2.800	2.800	2.800	2.800	2.800	2.800	2.800	2.800	2.800	2.800	2.800	2.800	2.800
M 13	4.920	4.920	4.920	4.920	4.920	4.920	4.920	4.920	4.920	4.920	4.920	4.920	7.380	7.380	7.380	7.380	7.380	7.380	7.380	7.380	7.380	9.840	9.840
M 14	1.804	1.804	1.804	1.804	1.804	1.804	1.804	1.804	1.804	1.804	1.804	1.804	1.804	1.804	1.804	1.804	1.804	1.804	1.804	1.804	1.804	1.804	1.804
M 15	1.838	1 838	1.838	1.838	1.838	1.838	1.838	1.838	1.838	1.838	1.838	1.838	1.838	1.838	1.838	1.838	1.838	1.838	1.838	1.838	1.838	1.838	3.676
M 16	1.360	1.360	1.360	1.360	1.360	1.360	1.360	1.360	1.360	1.360	1.360	1.360	1.360	1.360	1.360	1.360	1.360	1.360	1.360	1.360	1.360	1.360	1.360
Total Volume	20.873	20.873	23.673	23.673	24.680	26.680	26.680	26.680	26.680	26.680	26.680	26.680	29.140	31.484	31.484	34.284	34.284	34.284	34.284	35.291	35.291	37.751	41.589
Load/Volume	0.479	0.527	0.507	0.549	0.567	0.562	0.600	0.637	0.675	0.712	0.686	0.667	0.699	0.671	0.700	0.729	0.758	0.765	0.793	0.768	0.721		
Most Efficient	0.806	0.847	0.789	0.841	0.906	0.848	0.876	0.830	0.879	0.881	0.889	0.910	0.912	0.900	0.902	0.940	0.870	0.904	0.927	0.901	0.918		

TABLE 4. Strength of nodes and struts under design loads

	Node 1 (CCT)	Node 2 (TTT)	Node 3 (CTT)	Node 4 (CCT)	Node 5 (CCT)	Node 6 (TTT)	Node 7 (CTT)	Node 8 (CCC)	Node 9 (CTT)
Strength of Node (psi)	3060	2486	2486	3060	3060	2486	2486	3825	2486
Strength of Strut (psi)	2869	2869	2869	2869	2869	2869	2869	2869	2869
Usable Strength (psi)	2869	2486	2486	2869	2869	2486	2486	2869	2486

the usable strength, f_{ce}, in the calculation of the width of the struts/ties using the following equation:

$$w_t = \frac{P}{f_{ce} * 3.5\ in} \quad (4)$$

The width of all struts and ties for the specimen can be found in Table 5. For the 25-kip design loading the width of all struts and ties was found to be within the dimensions of the specimen, therefore, the full strength of the strut and tie layout could be utilized.

The selection of steel rebar for the model was based primarily on the number of possible bars that fit within the 3.5-inch thickness of the specimen. The maximum amount of any size bar that would fit was 3 bars, based on spacing and ease of placing the bars when constructing the specimen. Therefore, mostly No. 4 bars were used in high-stress areas such as members 9 and 13, which used 2 No. 4 and 3 No. 4 bars, respectively. A cross-section of the steel rebar layout used can be found in Figure 8. The efficiency of this rebar layout was 0.729 kips/volume, which is about 37% less than the most efficient layout calculated. This efficiency was found to be satisfactory due to the feasibility and ease of constructability parameters.

The steel layout was constructed using 5 continuous pieces of rebar. This procedure was done to ensure an effective amount of development length was present at each node. The continuation of rebar through most of the nodes also increased the stability and strength at the nodes.

TABLE 5. Width of struts and ties under design loads

Load (kips)	10	11	12	13	14	15	16	17	18	19	20	21	22	23	24	25	26	27	28	29	30
Member	**Width Of Strut/Tie (in)**																				
M1	0.434	0.477	0.521	0.564	0.607	0.651	0.694	0.738	0.781	0.824	0.868	0.911	0.954	0.998	1.041	1.085	1.128	1.171	1.215	1.258	1.302
M2	0.685	0.753	0.822	0.890	0.959	1.027	1.096	1.164	1.233	1.301	1.370	1.438	1.507	1.575	1.644	1.712	1.781	1.849	1.917	1.986	2.054
M3	0.183	0.201	0.219	0.238	0.256	0.274	0.293	0.311	0.329	0.347	0.366	0.384	0.402	0.421	0.439	0.457	0.475	0.494	0.512	0.530	0.549
M4	0.165	0.181	0.198	0.214	0.231	0.247	0.264	0.280	0.297	0.313	0.330	0.346	0.363	0.379	0.396	0.412	0.429	0.445	0.462	0.478	0.495
M5	1.183	1.301	1.419	1.538	1.656	1.774	1.892	2.011	2.129	2.247	2.366	2.484	2.602	2.720	2.839	2.957	3.075	3.194	3.312	3.430	3.548
M6	0.971	1.068	1.166	1.263	1.360	1.457	1.554	1.651	1.748	1.845	1.943	2.040	2.137	2.234	2.331	2.428	2.525	2.622	2.720	2.817	2.914
M7	0.802	0.882	0.962	1.042	1.122	1.202	1.282	1.363	1.443	1.523	1.603	1.683	1.763	1.844	1.924	2.004	2.084	2.164	2.244	2.324	2.405
M8	0.665	0.732	0.798	0.865	0.931	0.998	1.064	1.131	1.198	1.264	1.331	1.397	1.464	1.530	1.597	1.663	1.730	1.796	1.863	1.929	1.996
M9	0.780	0.858	0.937	1.015	1.093	1.171	1.249	1.327	1.405	1.483	1.561	1.639	1.717	1.795	1.873	1.951	2.029	2.107	2.185	2.263	2.341
M10	0.598	0.658	0.718	0.777	0.837	0.897	0.957	1.017	1.076	1.136	1.196	1.256	1.316	1.375	1.435	1.495	1.555	1 615	1.674	1.734	1.794
M11	0.263	0.290	0.316	0.342	0.369	0.395	0.421	0.448	0.474	0.500	0.527	0.553	0.579	0.606	0.632	0.658	0.685	0.711	0.737	0.764	0.790
M12	0.379	0.417	0.455	0.493	0.530	0.568	0.606	0.644	0.682	0.720	0.758	0.796	0.833	0.871	0.909	0.947	0.985	1.023	1.061	1.099	1.137
M13	0.937	1.031	1.124	1.218	1.312	1.405	1.499	1.593	1.687	1.780	1.874	1.968	2.061	2.155	2.249	2.342	2.436	2.530	2.624	2.717	2.811
M14	0.190	0.209	0.228	0.247	0.265	0.284	0.303	0.322	0.341	0.360	0.379	0.398	0.417	0.436	0.455	0.474	0.493	0.512	0.531	0.550	0.569
M15	0.309	0.340	0.370	0.401	0.432	0.463	0.494	0.525	0.556	0.587	0.617	0.648	0.679	0.710	0.741	0.772	0.803	0.834	0.864	0.895	0.926
M16	0.080	0.088	0.096	0.104	0.112	0.120	0.128	0.136	0.144	0.152	0.160	0.168	0.176	0.184	0.192	0.200	0.208	0.216	0.224	0.232	0.240
M17	0.273	0.300	0.327	0.355	0.382	0.409	0.437	0.464	0.491	0.518	0.546	0.573	0.600	0.628	0.655	0.682	0.710	0.737	0.764	0.791	0.819

*Light gray member denotes tension tie

3. RESULTS AND DISCUSSION

The experimental results were analyzed in terms of crack patterns, load deflection analysis, and load-to-steel weight ratio to find the efficiency of the antisymmetric reinforced concrete deep beams with openings under concentrated loading using the Strut and Tie Model. The following are the results obtained from the testing performed on the specimens.

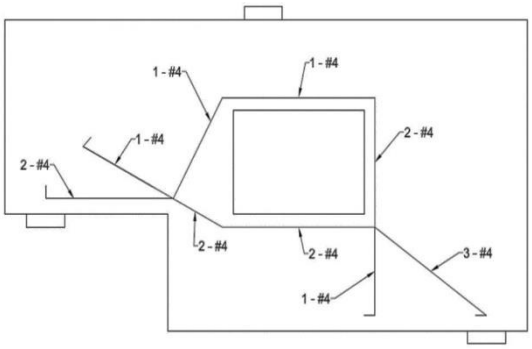

Figure 8. Steel rebar layout for the concrete specimen

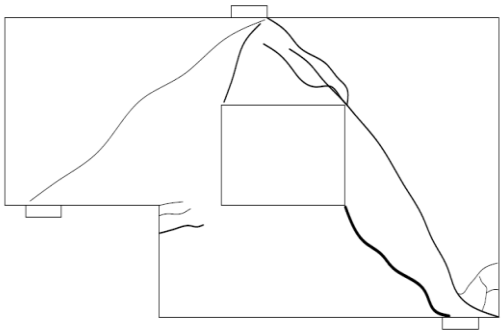

Figure 9. The crack pattern of Specimen 1 at failure

3.1. Crack Patterns In each structural element test, the crack patterns give an idea about the mode of failure. The failure mode and crack patterns are illustrated in Figures 9 to 12. The crack patterns induced on Specimen 1 were studied as shown in Figure 9. The first specimen showed a shear failure mode. At the early load stage, a visible crack was formed first at the bottom right support toward the applied point load. Cracking then began to form at the top left corner of the central opening. Once the cracking fully developed, shear failure rapidly occurred at the peak load as shown in Figure 10. Specimen 2 showed a local shear failure at two separate locations, at the top and bottom of the central opening. During the service load, a crack started from the point load and propagated to the top right corner of the central opening, resulting in local shear failure. A new crack then began to develop at the bottom of the specimen and progressed towards the central opening, creating the second area of local shear failure, as shown in Figure 11. The crack patterns for Specimen 3 were investigated and showed a flexural mode of failure with local shear failure. At the service load stage, a crack was formed at the bottom end of the specimen and propagated vertically toward the central opening. Many visible hairline cracks developed at the top left corner of the opening and went rapidly to the point load where crushing had already occurred in concrete beneath the bearing plate, as shown in Figure 12.

Figure 10. The failure mode in Specimen 1

Figure 11. The failure mode in Specimen 2

Figure 12. The failure mode in Specimen 3

3. 2. Load Deflection Analysis The load-deflection curve for all specimens was investigated. All specimens failed at peak loads lower than design loads, except Specimen 3. Load-deflection curves for each specimen showed an approximately linear response until the peak load. For Specimen 1, the ultimate load was 22 kips with 0.14-inch deflection, while its design capacity was 25 kips. The specimen exhibited a rapid drop at the peak load, which is an indication of shear failure. Specimen 2 achieved the highest peak load of 29.297 kips with 0.22 inches of deflection; however, the design load for this specimen was 35 kips. The specimen also shows a rapid loading drop after the peak load, resulting in a shear failure. The final Specimen 3 reached an ultimate load of 17.75 kips with 0.34 inches of deflection, which was

slightly greater than the design load of 17 kips. The progressive downward trend of the deflection after the peak load indicates the behavior of a flexural failure followed by local shear failure at the rapid drop in loading.

3. 3. Load to Steel Weight Ratio Efficiency in terms of load/weight of steel was the defining parameter in determining which specimen was the most effective. To establish the best reinforcement layout the weight of each specimen was calculated and divided by the ultimate load reached during testing. The weights for each type of reinforcement, flexural and shear, and the total reinforcement for each specimen, including the weight of the bar hooks, as summarized in Table 6.

Specimen 1 used the least amount of total reinforcement steel at 13.17 lb. This low weight was due to the exclusion of shear reinforcement in the steel design layout. Specimen 2 included shear reinforcement in the amount of 2.578 lb, but the flexural reinforcement of 17.189 lb amassed a total reinforcement weight of 19.767 lb. Specimen 3 used both flexural and shear reinforcement of 8.8 lb and 4.71 lb, respectively, measuring 13.51 lb of total reinforcement.

The specimen with the highest efficiency was Specimen 1 with a value of 1.67 kips/lb of steel. This specimen was 12.8% and 27.4% more efficient than Specimens 2 and 3, respectively. The efficiency for each specimen stated in Table 7.

TABLE 6. Weights of each type of reinforcement used in the strut and tie model for each specimen

Specimens	Flexural Reinforcement	Shear Reinforcement	Total Reinforcement
	Weight (1b)	Weight (1b)	Weight (1b)
1	13.170	0.000	13.170
2	17.189	2.578	19.767
3	8.800	4.710	13.510

TABLE 7. Load/weight ratio efficiencies for each specimen

Specimens	Reinforcement	Ultimate Load	Design Load	Deflection at	Efficiency
	(lb)	(kips)	(kips)	Ultimate (in)	(kips/lb)
1	13.170	22.000	25.000	0.140	1.670
2	19.767	29.297	35.000	0.220	1.480
3	13.510	17.750	16.000	0.340	1.310

4. CONCLUSIONS

1. It can be concluded that the efficient reinforcement layout of the strut and tie model leads to the highest efficiency of the model, regardless of the value of the externally applied load.
2. A comparison between the three specimens showed Specimen 1 had the highest efficiency of 1.67, while Specimen 3 had the lowest efficiency of 1.31. Specimen 1 reached 88% of its designed load, while Specimen 2 reached 83.7% of its design load.
3. By looking at the mode failure of Specimen 1, which failed due to shear, if the specimen included shear reinforcement, the design load may have been attained.
4. Due to the exclusion of shear reinforcement in Specimen 1, the ductility of the specimen was much lower compared to the other specimens.
5. All specimens were within the serviceability limit for deflection of 0.48 inches. The deflection of Specimen 1 was 57% less than Specimen 2 and 143% less than Specimen 3. The lack of ductility in this specimen leads to brittle failure.
6. From the analysis of these results, it is clear that the strut and tie model of Specimen 1 would have provided reasonable ductility for the applied load if shear reinforcement had been added to the deeper section of the specimen.
7. Based on the results of the research, reinforcement of antisymmetric reinforced concrete deep beams can be designed. Fundamental tests of at least 20 samples must be done before the production of the respective ones.

5. REFERENCES

1. Shear, A.-A.C.o. and Torsion, "Recent approaches to shear design of structural concrete", ***Journal of Structural Engineering***, Vol. 124, No. 12, (1998), 1375-1417, https://doi.org/10.1061/(ASCE)0733-9445(1998)124:12(1375)
2. "American association of state highway officials and transportation (aashto), "lrfd bridge design specifications. 7th edition ed."", in AASHTO, Washington, DC, (2014 of Conference).
3. Committee, A., "Building code requirements for structural concrete (aci 318-08) and commentary, American Concrete Institute. (2008).
4. Association, C.S., "Design of concrete structures (csa a23. 3-04)", ***CSA, Rexdale, Ontario***, (2004).
5. Institution, B.S., "Eurocode 2: Design of concrete structures: Part 1-1: General rules and rules for buildings, British Standards Institution, (2004).
6. Taerwe, L. and Matthys, S., *Fib model code for concrete structures 2010*. 2013, Ernst & Sohn, Wiley.
7. Ritter, W., "The hennebique design method (die bauweise hennebique)", ***Schweizerische Bauzeitung (Zurich)***, Vol. 33, No. 7, (1899), 59-61.

8. Mörsch, E., "Concrete-steel construction:(der eisenbetonbau), Engineering news publishing Company, (1909).
9. Schlaich, J., Schäfer, K. and Jennewein, M., "Toward a consistent design of structural concrete", ***PCI journal***, Vol. 32, No. 3, (1987), 74-150.
10. Schlaich, J. and Schafer, K., "Design and detailing of structural concrete using strut-and-tie models", ***Structural Engineer***, Vol. 69, No. 6, (1991), 113-125.
11. Xie, Y.M. and Steven, G.P., "A simple evolutionary procedure for structural optimization", ***Computers & Structures***, Vol. 49, No. 5, (1993), 885-896, https://doi.org/10.1016/0045-7949(93)90035-C.
12. Yang, X.Y., Xie, Y.M., Steven, G.P. and Querin, O., "Bidirectional evolutionary method for stiffness optimization", ***AIAA Journal***, Vol. 37, No. 11, (1999), 1483-1488, https://doi.org/10.2514/2.626
13. Liang, Q.Q., Xie, Y.M. and Steven, G.P., "Topology optimization of strut-and-tie models in reinforced concrete structures using an evolutionary procedure", ***Structural Journal***, Vol. 97, No. 2, (2000), 322-330.
14. Liang, Q.Q., Xie, Y.M. and Steven, G.P., "Generating optimal strut-and-tie models in prestressed concrete beams by performance-based optimization", ***ACI Structural Journal***, Vol. 98, No. 2, (2001), 226-232.
15. Cai, C.S., "Three-dimensional strut-and-tie analysis for footing rehabilitation", ***Practice Periodical on Structural Design and Construction***, Vol. 7, No. 1, (2002), 14-25, https://doi.org/10.1061/(ASCE)1084-0680(2002)7:1(14)
16. Leu, L.-J., Huang, C.-W., Chen, C.-S. and Liao, Y.-P., "Strut-and-tie design methodology for three-dimensional reinforced concrete structures", ***Journal of Structural Engineering***, Vol. 132, No. 6, (2006), 929-938, https://doi.org/10.1061/(ASCE)0733-9445(2006)132:6(929)
17. Nagarajan, P. and Pillai, T.M., "Development of strut and tie models for simply supported deep beams using topology optimization", ***Sonklanakarin Journal of Science and Technology***, Vol. 30, No. 5, (2008), 641.
18. Bruggi, M., "Generating strut-and-tie patterns for reinforced concrete structures using topology optimization", ***Computers & Structures***, Vol. 87, No. 23-24, (2009), 1483-1495, https://doi.org/10.1016/j.compstruc.2009.06.003
19. Guest, J.K., "Imposing maximum length scale in topology optimization", ***Structural and Multidisciplinary Optimization***, Vol. 37, (2009), 463-473, https://doi.org/10.1007/s00158-008-0250-7
20. Guest, J.K. and Moen, C.D., "Reinforced concrete design with topology optimization", in Structures Congress 2010: 19th Analysis and Computation Specialty Conference. (2010), 445-454. https://doi.org/10.1061/41131(370)39
21. Herranz, J.P., Santa María, H., Gutierrez, S. and Riddell, R., "Optimal strut-and-tie models using full homogenization optimization method", ***ACI Structural Journal***, Vol. 109, No. 5, (2012), 605.
22. Almeida, V.S., Simonetti, H.L. and Neto, L.O., "Comparative analysis of strut-and-tie models using smooth evolutionary structural optimization", ***Engineering Structures***, Vol. 56, (2013), 1665-1675, https://doi.org/10.1016/j.engstruct.2013.07.007
23. Palmisano, F. and Elia, A., "Shape optimization of strut-and-tie models in masonry buildings subjected to landslide-induced settlements", ***Engineering Structures***, Vol. 84, (2015), 223-232, https://doi.org/10.1016/j.engstruct.2014.11.030
24. Palmisano, F., Alicino, G. and Vitone, A., "Nonlinear analysis of rc discontinuity regions by using the bi-directional evolutionary structural optimization method", in Proc. of the OPT-I, An International Conference on Engineering and Applied Sciences Optimization. (2014), 749-758.
25. Bruggi, M., "A numerical method to generate optimal load paths in plain and reinforced concrete structures", ***Computers & Structures***, Vol. 170, (2016), 26-36, https://doi.org/10.1016/j.compstruc.2016.03.012
26. El-Metwally, S. and Chen, W.-F., "Structural concrete: Strut-and-tie models for unified design, CRC Press, (2017).
27. Chen, H., Yi, W.-J. and Hwang, H.-J., "Cracking strut-and-tie model for shear strength evaluation of reinforced concrete deep beams", ***Engineering Structures***, Vol. 163, (2018), 396-408, https://doi.org/10.1016/j.engstruct.2018.02.077
28. Geevar, I. and Menon, D., "Strength of reinforced concrete pier caps-experimental validation of strut-and-tie method", ***ACI Structural Journal***, Vol. 116, No. 1, (2019).
29. Al-Ameri, A., Jawad, F. and Fattah, M., "Vertical and lateral displacement response of foundation to earthquake loading", ***International Journal of Engineering, Transactions A: Basics***, Vol. 33, No. 10, (2020), 1864-1871, doi: 10.5829/IJE.2020.33.10A.05.
30. Hussein, A., Al-Neami, M. and Rahil, F., "Effect of hydrodynamic pressure on saturated sand supporting liquid storage tank during the earthquake", ***International Journal of Engineering, Transactions B: Applications***, Vol. 34, No. 5, (2021), 1176-1183, doi: 10.5829/IJE.2021.34.05B.11.
31. Xia, Y., Langelaar, M. and Hendriks, M.A., "Automated optimization-based generation and quantitative evaluation of strut-and-tie models", ***Computers & Structures***, Vol. 238, (2020), 106297, https://doi.org/10.1016/j.compstruc.2020.106297
32. Xia, Y., Langelaar, M. and Hendriks, M.A., "Optimization-based three-dimensional strut-and-tie model generation for reinforced concrete", ***Computer-Aided Civil and Infrastructure Engineering***, Vol. 36, No. 5, (2021), 526-543, https://doi.org/10.1111/mice.12614
33. Xia, Y., Langelaar, M. and Hendriks, M.A., "Optimization-based strut-and-tie model generation for reinforced concrete structures under multiple load conditions", ***Engineering Structures***, Vol. 266, (2022), 114501, https://doi.org/10.1016/j.engstruct.2022.114501
34. Kassem, M.M., Nazri, F.M., Farsangi, E.N. and Ozturk, B., "Improved vulnerability index methodology to quantify seismic risk and loss assessment in reinforced concrete buildings", ***Journal of Earthquake Engineering***, Vol. 26, No. 12, (2022), 6172-6207, https://doi.org/10.1080/13632469.2021.1911888
35. Kassem, M.M., Nazri, F.M., Farsangi, E.N. and Ozturk, B., "Development of a uniform seismic vulnerability index framework for reinforced concrete building typology", ***Journal of Building Engineering***, Vol. 47, (2022), 103838, https://doi.org/10.1016/j.jobe.2021.103838
36. Jabbar, A.M., Mohammed, D.H. and Hasan, Q.A., "A numerical study to investigate shear behavior of high-strength concrete beams externally retrofitted with carbon fiber reinforced polymer sheets", ***International Journal of Engineering, Transactions B: Applications,***, Vol. 36, No. 11, (2023), 2112-2123, doi: 10.5829/IJE.2023.36.11B.15.
37. Mohammed, A., Al-Zuheriy, A. and Abdulkareem, B., "An experimental study to predict a new formula for calculating the deflection in wide concrete beams reinforced with shear steel plates", ***International Journal of Engineering, Transactions B: Applications***, Vol. 36, No. 2, (2023), 360-371, doi: 10.5829/IJE.2023.36.02B.15.
38. Chaudhari, A.D. and Suryawanshi, S., "Development and calibration of an efficiency factor model for recycled aggregate concrete struts", ***International Journal of Engineering, Transactions B: Applications***, Vol. 36, No. 8, (2023), 1449-1458, doi: 10.5829/IJE.2023.36.08B.05.

Persian Abstract

چکیده

تکنیک مدل‌سازی (STM) یک روش کاربردی و ارزشمند برای مهندسان سازه برای طراحی مناطق آشفته-D مناطق سازه‌های بتن مسلح است که در آن فرض باقی‌مانده مقاطع صفحه پس از بارگذاری غیرقابل اجرا است. مهمترین جنبه برای تضمین عملکرد مناسب سازه ای و اقتصادی طرح، یافتن یک مدل قیاسی خرپایی مناسب است که منجر به استفاده از مدل کارآمدتر در ساختمان های سازه می شود. ارزیابی مدل‌های ضد متقارن(STM) با دهانه‌های تحت بارهای خارجی متمرکز مختلف به طور جامع در ادبیات بررسی نشده است. بنابراین، برای پرداختن به این شکاف، هدف این مقاله دستیابی به کارآمدترین طرح آرماتور در تیرهای عمیق بتن مسلح ضد متقارن با بازشوهای تحت بارگذاری متمرکز با استفاده از مدل پایه و کراوات است. کار آزمایشی انجام شد و شامل (۳) تیرهای عمیق بتن مسلح ضد متقارن با دهانه‌هایی بود که تحت بارهای متمرکز مختلف (به ترتیب ۲۵، ۳۵، و ۱۶ کیپس برای نمونه‌های ۱، ۲ و ۳) با استفاده از مدل پایه و کراوات آزمایش شدند. نرم افزار ANSYS FEM برای آنالیز پایه و کراوات اولیه و برنامه تحلیل سازه RISA-3D برای یافتن نیروهای داخلی برای همه اعضا تحت بارهای خارجی متمرکز در هر نمونه استفاده می شود. یافته‌های این مقاله نشان می‌دهد که نمونه ۱ با ۱/۶۷ بیشترین بازده و نمونه ۳ با ۱/۳۱ کمترین راندمان را داشته است. می‌توان نتیجه گرفت که چیدمان تقویت‌کننده کارآمد مدل پایه و کراوات بدون در نظر گرفتن مقدار بار اعمال‌شده خارجی، منجر به بالاترین بازده مدل می‌شود.